Electronic Supplementary Information (ESI)

Hypso- or bathochromic phosphorescent mechanochromic mononuclear Cu(I) complexes with a bis(2-diphenylphosphinophenyl)ether auxiliary ligand

Hai-feng He,[a]* Jia-kun Zhang,[a] Xiao-yun Wu,[a] Feng Zhao,[a]* Yu-zhen Huang,[a] Ming-cong Wang,[a] Chao-xuan Feng,[a] De-rui Mao,[a] Xue-long Huang,[b]* Yi-fan Hu,[a]

[a] *Jiangxi Provincial Engineering Research Center for Waterborne Coatings, School of Chemistry and Chemical Engineering, Jiangxi Science and Technology Normal University, Nanchang 330013, People's Republic of China*

[b] *College of Medical Information·Engineering, Gannan Medical University, Ganzhou 341000, People's Republic of China*

* Corresponding author E-mail: hehf0427@jxstnu.com.cn; zhf19752003@163.com; huangxuelong@gmu.edu.cn

General: All chemical reagents can be obtained from the available commercial sources. ^{1}H NMR and ^{13}C NMR spectra were obtained by a Bruker AV400 MHz spectrometer. UV-vis absorption spectra of Cu(I) complexes **1** and **2** were obtained on an Agilent 8453 UV/Vis spectrophotometer. Hitachi F-4600 fluorescence spectrophotometer was employed to measure the emission spectra of complexes **1**-**6**. The absolute PL quantum yields of complexes **1**-**6** in various solid states were determined by a FLS980 fluorescence spectrophotometer (Edinburgh Instruments Ltd., U. K.) using an integrating sphere and a continuous xenon lamp (450 W) as an excitation source. The PL lifetimes were measured by the FLS980 spectrofluorometer using a microsecond light source. Mass spectra data were collected by Waters ACQUITY UPLC H-CLASS PDA (Waters). Density functional theory (DFT) calculations were carried out at the B3LYP/6-31G* level with the Gaussian 09 program, and the LANL2DZ basis set was applied for the copper atom and 6-31G(d) for the others. XRD studies of complexes **1**-**6** were recorded on a Shimadzu XRD-6000 diffractometer (Japan) (Cu Kα, 40 kV and 30 mA). X-ray crystal structures of complexes **1**-**4** and **6** were obtained on a Bruker APEX DUO CCD system (Germany), and their structures were fully analyzed by a combination of direct methods (SHELXS-97) and fourier difference techniques and refined by full-matrix least-squares (SHELXL-97), and their crystallographic data of complexes **1**-**4** and **6** were deposited in the Cambridge Crystallographic Data Centre as supplemental publication CCDC 2222884 (complex **1**), CCDC 2222885 (complex **2**), CCDC 2222887 (complex **3**), CCDC 2222888 (complex **4**), CCDC 2222889 (complex **6**).

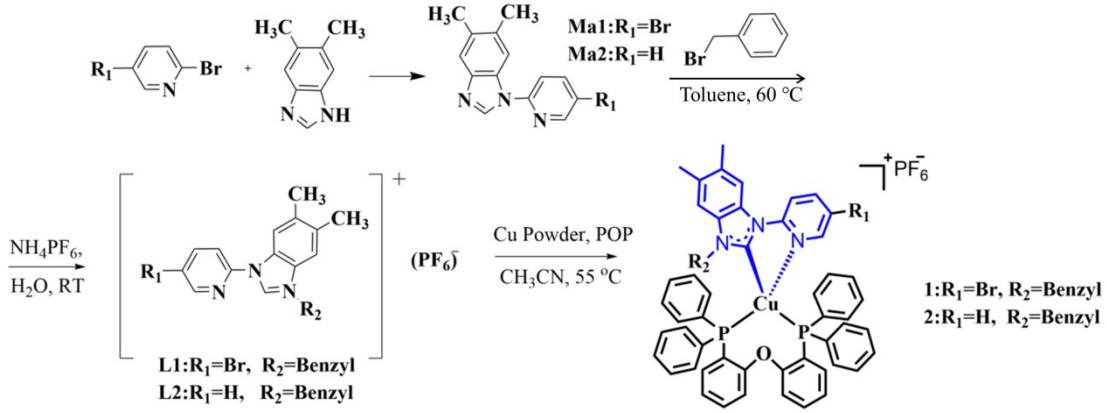

Scheme S1. Synthetic route for Cu(I) complexes **1** and **2**.

*General syntheses for Cu(I) complexes **1** and **2**.*

The synthetic procedures of Cu(I) complexes **1** and **2** are shown in Scheme S1 (Supporting information).

*General syntheses for intermediates **Ma1, Ma2:*** 2,5-dibromopyridine (1.88 g, 8 mmol) or 2-bromopyridine (1.26 g, 8 mmol), 5, 6-dimethyl-benzimidazole (1.46 g, 10 mmol), sodium tert-butoxide (0.96 g, 10 mmol), and 20 mL DMSO were added to three-necked bottle, finally CuI (0.15 g, 0.8 mmol) was added. And then, the mixture was stirred for 12 h under N_2 at 110 °C. After the reaction was completed by TLC detection, the reaction solution was poured into 150 mL ice water, and extracted with ethyl acetate. The organic phase was washed with saturated salt solution, dried with $MgSO_4$ and filtered, respectively. Then, the mixture evaporated under reduced pressure and without further purification is used for the next step.

*General syntheses for ligands **L1** and **L2**:* **Ma1** (2.41 g, 8 mmol), benzyl bromide (1.64 g, 9.6 mmol) and 20 mL toluene were added to three-necked bottle, and refluxed for 24 h at 110 °C. After the reaction is completed, and cooled to room

temperature, white solid was obtained by filtering. After NH_4PF_6 was added to the methanol solution of white solid, a large amount of white precipitate was generated and filtrated to obtain pure white solid **L1**. The synthesis and purification processes of **L2** are similar to **L1**.

*General syntheses for **1** and **2:*** **L1** (0.537 g, 1 mmol), Cu powder (0.077 g, 1.2 mmol), POP (0.55 g, 1 mmol) and 25 mL CH_3CN were added to 100 mL round–bottomed flask and reacted overnight at 55 °C. The mixed solution was passed through silica and evaporated at reduced pressure to remove the solvent. Then ethanol was added to the crude product and stirred for 1 h at 60 °C to obtain a light yellow pure product **1**. The synthesis and purification processes of **2** are similar to **1**.

For **1,** faint yellow solid; yield (64.4%); ^{1}H NMR (400 MHz, DMSO-d_6) δ (ppm) 2.25 (s, 3H, CH_3), 2.41 (s, 3H, CH_3), 5.39 (s, 2H, CH_2), 6.57 (s, 2H, POP-H), 6.84 (d, J = 8.0 Hz, 6H, POP-H), 6.94 (d, J = 7.5 Hz, 2H, POP-H), 7.08 (dd, J = 13.9, 6.8 Hz, 7H, POP-H), 7.19-7.28 (m, 11H, POP-H), 7.32-7.44 (m, 6H, Ar-H), 7.86 (s, 1H, Py-H), 8.15 (s, 1H, Py-H), 8.28 (d, J = 8.8 Hz, 1H, Ar-H), 8.39 (d, J = 8.8 Hz, 1H, Py-H); ^{13}C NMR (101 MHz, DMSO-d_6) δ(ppm) 158.1, 149.8, 149.1, 143.2, 135.4, 134.4, 134.2, 134.1, 133.5, 132.9, 132.7, 131.1, 130.8, 130.5, 130.0, 129.3, 129.0, 128.0, 126.8, 125.8, 123.6, 123.4, 123.3, 120.8, 117.4, 116.2, 114.2, 113.1, 52.5, 20.3, 20.1; LC-MS (m/z, ES$^+$): calcd. For $C_{57}H_{46}BrCuN_3OP_2$ ([M]$^+$) 992.16; found 992.39. For **2,** faint yellow solid; yield (68.6%); ^{1}H NMR (400 MHz, DMSO-d_6) δ (ppm) 2.26 (s, 3H, CH_3), 2.42 (s, 3H, CH_3), 5.23 (s, 2H, CH_2), 6.59 (s, 2H, POP-H), 6.78 (d, J = 7.6 Hz, 2H, POP-H), 6.88-6.99 (m, 10H, POP-H), 7.06 (dd, J = 13.2, 5.8 Hz, 3H, POP-H, Ar-

H), 7.16-7.29 (m, 12H, POP-H), 7.30-7.46 (m, 7H, Ar-H), 8.12 (dd, J = 18.3, 6.1 Hz, 2H, Py-H), 8.21 (s, 1H, Py-H), 8.46 (d, J = 8.4 Hz, 1H, Py-H); ^{13}C NMR (101 MHz, DMSO-d_6) δ(ppm) 158.3, 158.2, 151.0, 148.9, 141.4, 135.5, 134.3, 134.3, 134.2, 134.0, 133.1, 133.1, 132.8, 131.9, 131.8, 130.5, 130.1, 129.3, 128.9, 127.9, 126.6, 125.6, 123.7, 123.0, 120.9, 114.7, 114.2, 113.0, 52.2, 20.3, 20.1; calcd. For $C_{57}H_{47}CuN_3OP_2$ ([M]$^+$) 914.25; found 914.59.

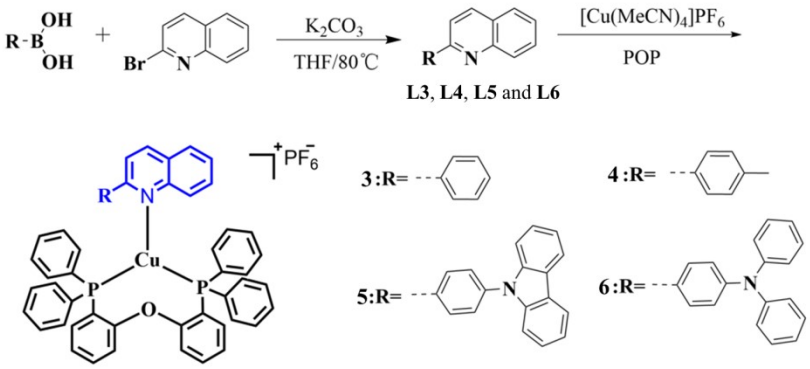

Scheme S2. Synthetic route for Cu(I) complexes **3**-**6**.

*General syntheses for Cu(I) complexes **3-6**.*

The synthetic procedures of Cu(I) complexes **3**-**6** are shown in Scheme S2 (Supporting information).

*General syntheses for ligands **L3**, **L4**, **L5** and **L6**:* 2-bromoquinoline (2.08 g, 10 mmol), phenylboronic acid (1.22 g, 10 mmol), tetrakis(triphenylphosphine)palladium (0.58 g, 0.5 mmol), 20 mL tetrahydrofuran and 20 mL K_2CO_3 (2 mol/L) were added to a 100 mL round-bottomed flask, respectively. The mixture was stirred at 85 °C under nitrogen for 8h. And then, cool water (100 mL) was added to the mixture, and extracted with dichloromethane, dried over anhydrous magnesium sulfate and filtered. The solvent was evaporated under reduced pressure to get the crude extract. The crude

extract was purified by recrystallizing from dichloromethane to obtain ligand **L3**. The synthesis and purification processes of **L4, L5** and **L6** are similar to **L3**.

*General syntheses for **3-6:*** $[Cu(MeCN)_4]PF_6$ (0.74 g, 2 mmol), POP (1.08 g, 2 mmol) and 10 mL dichloromethane were mixed in a 100 mL round-bottomed flask under nitrogen with stirring at room temperature for 1 h, and 10 mL dichloromethane solution of 2-phenylquinoline (0.41 g, 2 mmol) was added to the mixture with further stirring at room temperature for 3 h. The crude product was obtained by filtering the mixture through a plug of diatomite and concentrating. The pale white solid **3** was obtained by washed and recrystallized with Et_2O. The synthesis and purification processes of **4, 5** and **6** are similar to **3**. For **3**, white solid; yield (61.3%); ^{1}H NMR (400 MHz, DMSO-d_6) δ (ppm) 6.60-6.72 (m, 2H, POP-H), 7.04 (dd, J = 14.3, 7.5 Hz, 4H, POP-H), 7.33 (d, J = 5.9 Hz, 10H, POP-H), 7.44 (d, J = 6.5 Hz, 12H, POP-H), 7.50-7.62 (m, 4H. Ar-H), 7.76-7.80 (m, 1H, Ar-H), 8.01 (d, J = 8.1 Hz, 1H, Quinolone-H), 8.08 (d, J = 8.4 Hz, 1H, Quinolone-H), 8.16 (d, J = 8.6 Hz, 1H, Quinolone-H), 8.27-8.29 (m, 2H, Quinolone-H), 8.47 (d, J = 8.6 Hz, 1H, Quinolone-H); ^{13}C NMR (101 MHz, DMSO-d_6) δ (ppm) 157.4, 156.1, 147.5, 138.6, 137.2, 133.7, 133.5, 133.4, 133.4, 131.9, 131.2, 131.1, 130.9, 130.3, 129.9, 129.6, 129.0, 128.8, 127.8, 127.2, 126.4, 124.9, 123.5, 123.4, 123.2, 120.2, 118.75; calcd. For $C_{51}H_{39}CuNOP_2$ ($[M]^+$) 806.18; found 806.29. For **4**, white solid; yield (43.2%); ^{1}H NMR (400 MHz, DMSO-d_6) δ (ppm) 2.39(s, 3H, CH_3), 6.65 (s, 2H, POP-H), 7.04 (dd, J = 14.7, 7.4 Hz, 4H, POP-H), 7.32-7.37 (m, 12H, POP-H), 7.45 (d, J = 6.0 Hz, 12H, POP-H, Ar-H), 7.58 (t, J = 7.5 Hz, 1H, Ar-H)), 7.73-7.82 (m, 1H, Ar-H), 7.99 (d, J =

8.1 Hz, 1H, Quinolone-H), 8.06 (d, *J* = 8.4 Hz, 1H, Quinolone-H), 8.13 (d, *J* = 8.7 Hz, 1H, Quinolone-H), 8.19 (d, *J* = 8.2 Hz, 2H, Quinolone-H), 8.44 (d, *J* = 8.7 Hz, 1H, Quinolone-H); ^{13}C NMR (101 MHz, DMSO-d_6) δ (ppm) 157.9, 156.6, 148.0, 139.7, 137.5, 136.4, 134.2, 134.0, 133.9, 133.8, 132.4, 131.8, 131.6, 131.4, 130.7, 130.3, 129.9, 129.4, 129.3, 128.2, 127.6, 127.4, 126.7, 125.3, 123.9, 120.6, 119.0, 21.3; calcd. For $C_{52}H_{41}CuNOP_2$ ($[M]^+$) 820.20; found 820.17. For **5**, light grey solid; yield (45.8%); ^{1}H NMR (400 MHz, DMSO-d_6) δ (ppm) 6.65 (s, 2H, POP-H), 6.96-7.10 (m, 4H, POP-H), 7.20-7.24 (m, 2H, Carbazole-H), 7.32(s, 11H, POP-H), 7.44(s, 13H, POP-H, Carbazole-H), 7.52-7.59 (m, 3H, Ar-H), 7.63 (d, *J* = 8.3 Hz, 2H, Carbazole-H), 7.76 (t, *J* = 7.1 Hz, 1H, Ar-H), 7.98 (d, *J* = 7.8 Hz, 1H, Quinolone-H), 8.09 (d, *J* = 8.2 Hz, 1H, Quinolone-H), 8.28 (dd, *J* = 14.7, 8.2 Hz, 2H, Quinolone-H), 8.44 (t, *J* = 8.8 Hz, 2H, Quinolone-H), 9.07 (s, 1H, Carbazole-H) , 11.51 (s, 1H, Carbazole-H); ^{13}C NMR (101 MHz, DMSO-d_6) δ (ppm) 157.9, 157.6, 148.2, 141.3, 140.8, 137.3, 134.2, 134.0, 133.9, 133.8, 132.4, 131.7, 131.6, 131.4, 130.7, 130.2, 130.0, 129.3, 128.2, 127.1, 126.4, 126.3, 125.6, 125.3, 124.0, 123.9, 123.7, 123.4, 123.3, 120.9, 120.6, 119.9, 119.5, 119.2, 111.7; calcd. For $C_{63}H_{46}CuN_2OP_2$ ($[M]^+$) 971.24; found 971.44. For **6**, yellow solid; yield (41.3%); ^{1}H NMR (400 MHz, DMSO-d_6) δ (ppm) 6.56-6.72 (m, 2H, POP-H), 6.95-6.17 (m, 12H, POP-H), 7.32-7.38 (m, 14H, POP-H), 7.44 (d, *J* = 6.7 Hz, 12H, Triphenylamine-H), 7.56 (t, *J* = 7.4 Hz, 1H, Triphenylamine-H), 7.74 (t, *J* = 7.6 Hz, 1H, Triphenylamine-H), 7.99 (dd, *J* = 19.0, 8.1 Hz, 2H, Quinolone-H), 8.07 (d, *J* = 8.7 Hz, 1H, Quinolone-H), 8.18 (d, *J* = 8.7 Hz, 2H, Quinolone-H), 8.40 (d, *J* = 8.7 Hz, 1H, Quinolone-H); ^{13}C NMR (101 MHz,

DMSO-d_6) δ (ppm) 157.9, 156.1, 149.2, 148.1, 147.2, 137.4, 134.2, 134.0, 133.9, 133.8, 132.4, 131.8, 131.6, 131.4, 130.7, 130.3, 130.2, 129.3, 128.8, 128.2, 127.2, 126.5, 125.3, 125.2, 124.2, 124.0, 123.9, 123.8, 122.4, 120.6, 118.8; calcd. For $C_{63}H_{48}CuN_2OP_2$ ([M]$^+$) 973.25; found 973.48.

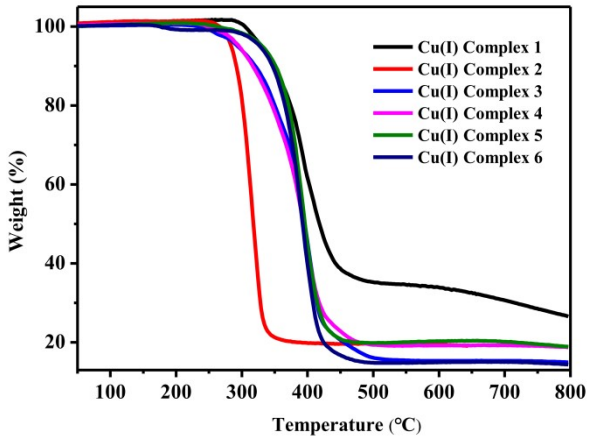

Fig. S1. TGA thermograms of Cu(I) complexes **1**-**6**.

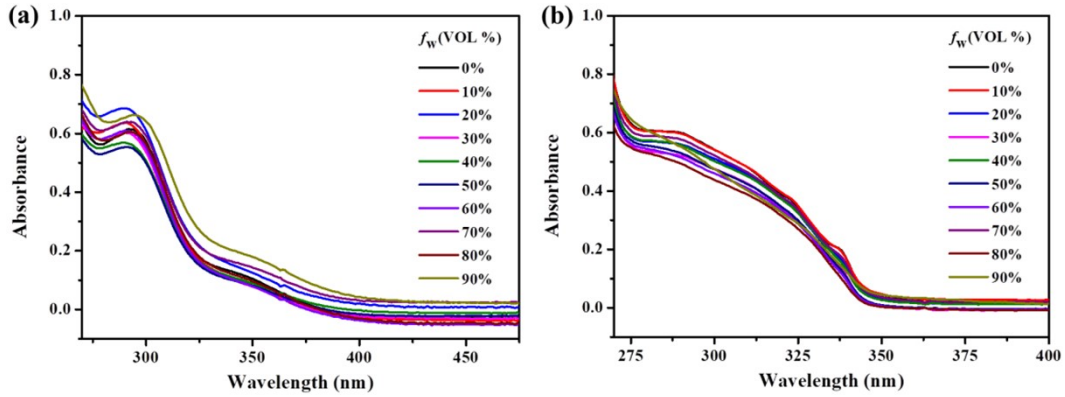

Fig. S2. UV-vis absorption spectra of Cu(I) complexes **1** (a) and **2** (b) in DMF/H_2O mixtures with varying water content (0%-90%). Concentration: 20 μM.

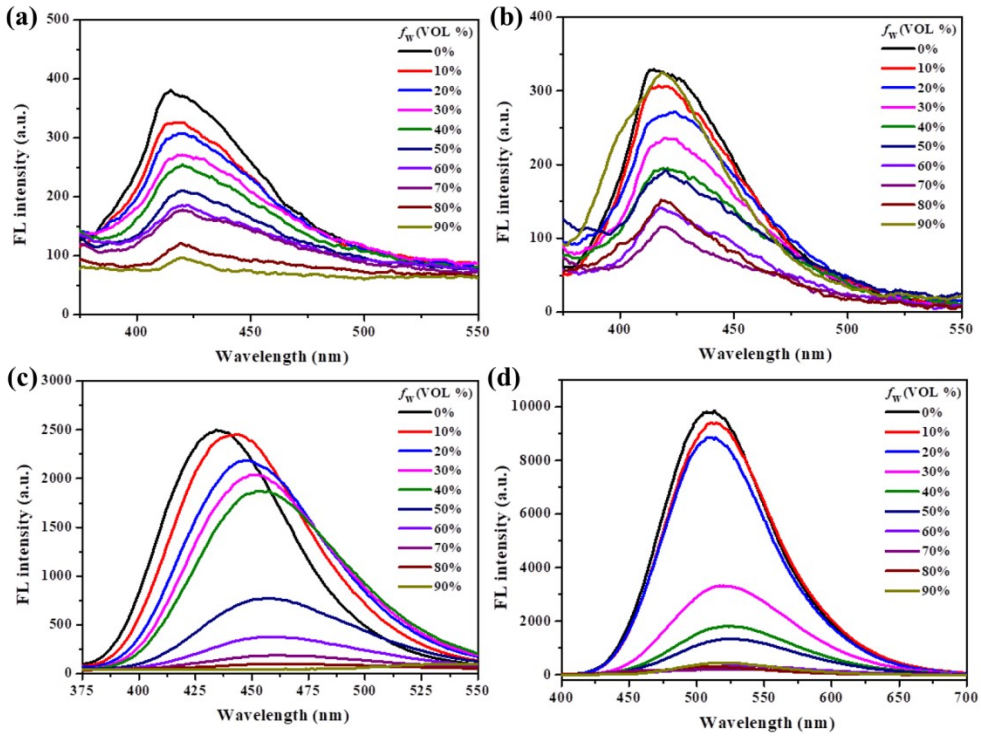

Fig. S3. PL spectra of Cu(I) complexes **3** (a), **4** (b), **5** (c) and **6** (d) in DMF/H_2O mixtures with varying water content (0%-90%). Concentration: 20 μM. Excitation wavelength: 365 nm.

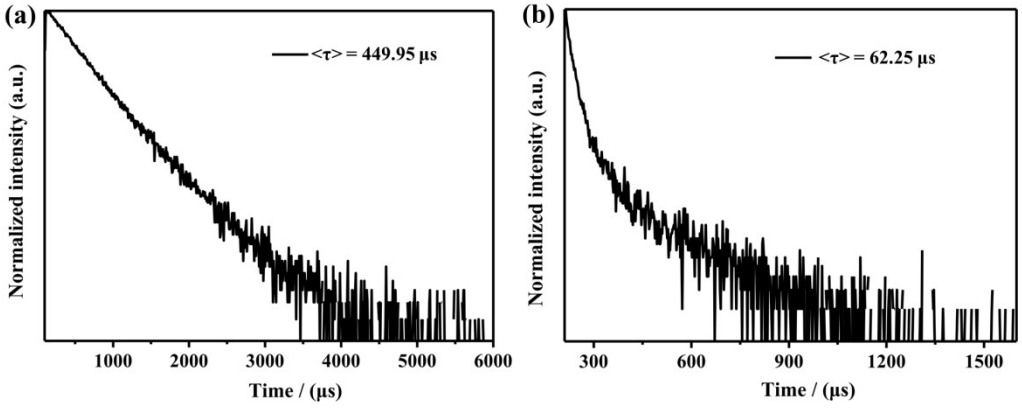

Fig. S4. (a) PL decay curve of unground Cu(I) complex **5** (567 nm). Excitation wavelength: 365 nm. (b) PL decay curve of ground Cu(I) complex **5** (551 nm). Excitation wavelength: 365 nm.

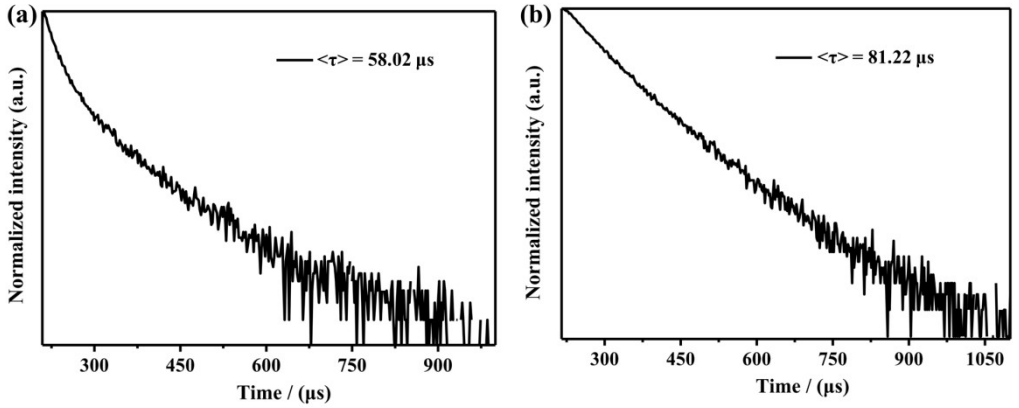

Fig. S5. (a) PL decay curve of unground Cu(I) complex **3** (536 nm). Excitation wavelength: 365 nm. (b) PL decay curve of ground Cu(I) complex **3** (570 nm). Excitation wavelength: 365 nm.

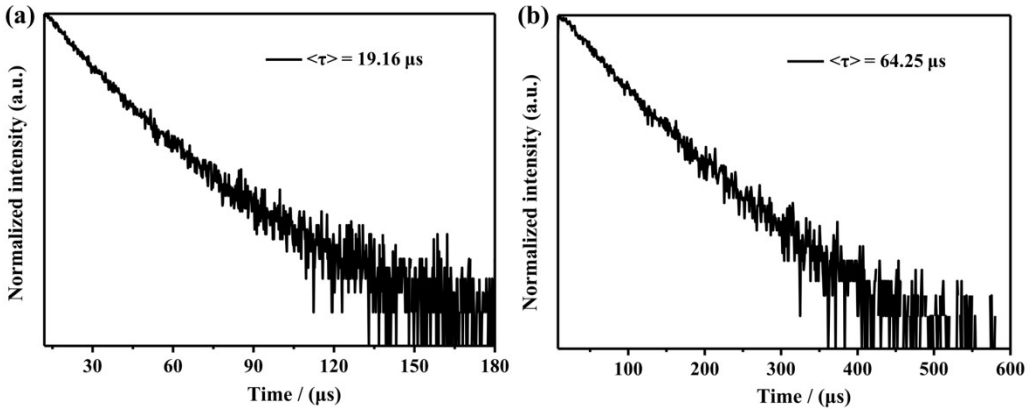

Fig. S6. (a) PL decay curve of unground Cu(I) complex **4** (539 nm). Excitation wavelength: 365 nm. (b) PL decay curve of ground Cu(I) complex **4** (560 nm). Excitation wavelength: 365 nm.

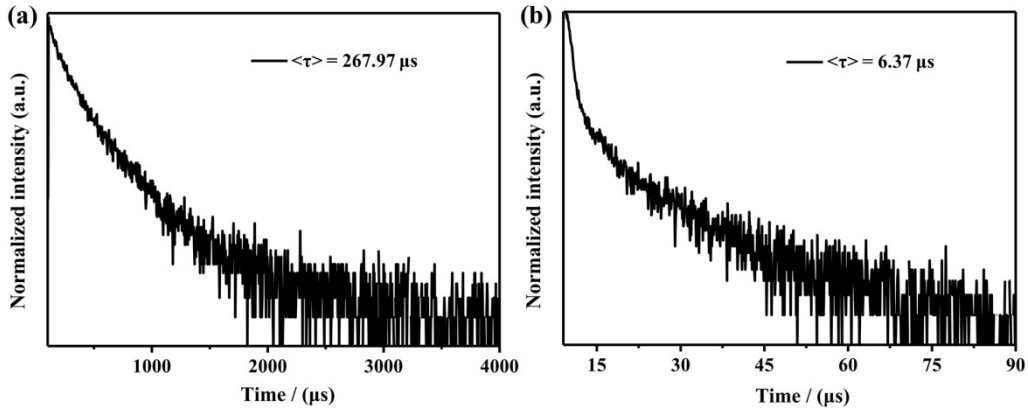

Fig. S7. (a) PL decay curve of unground Cu(I) complex **6** (549 nm). Excitation wavelength: 365 nm. (b) PL decay curve of ground Cu(I) complex **6** (586 nm). Excitation wavelength: 365 nm.

Table S1. PL quantum yields and PL lifetimes of Cu(I) complexes **1**-**6** before and after grinding. Excitation wavelength: 365 nm.

Cu(I) complex	PL quantum yield (Φ) of pristine solid	PL quantum yield (Φ) of ground solid	PL lifetime (<τ>) of pristine solid	PL lifetime (<τ>) of ground solid
1	21%	12%	16.13 μs	15.52 μs
2	30%	22%	41.46 μs	26.57 μs
3	16%	16%	58.02 μs	81.22 μs
4	10%	16%	19.16 μs	64.25 μs
5	24%	16%	449.95 μs	62.25 μs
6	39%	24%	267.97 μs	6.37 μs

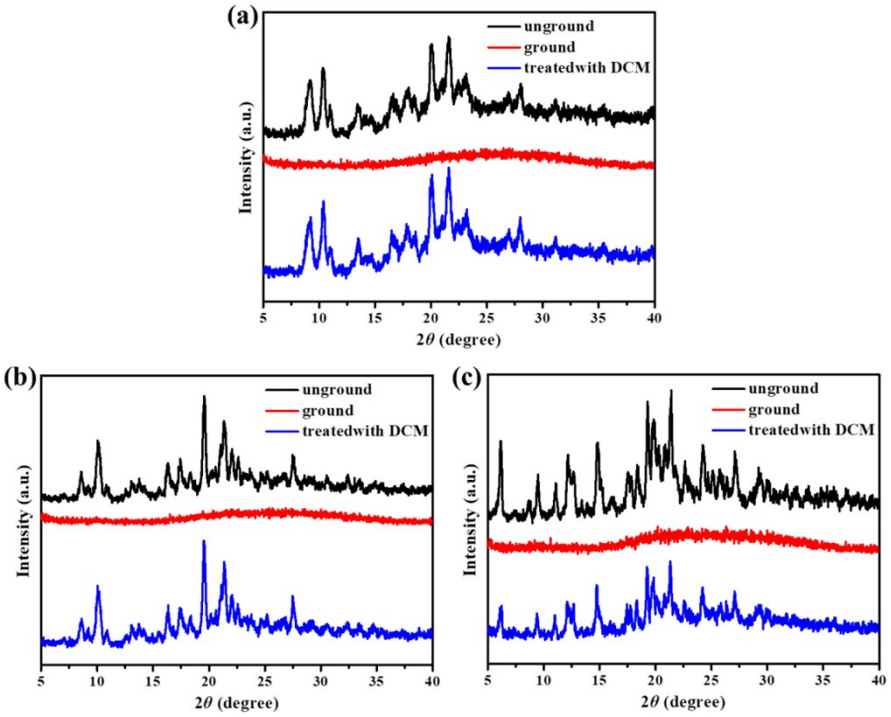

Fig. S8. Powder XRD patterns of Cu(I) complexes **3** (a), **4** (b) and **6** (c) in different solid states.

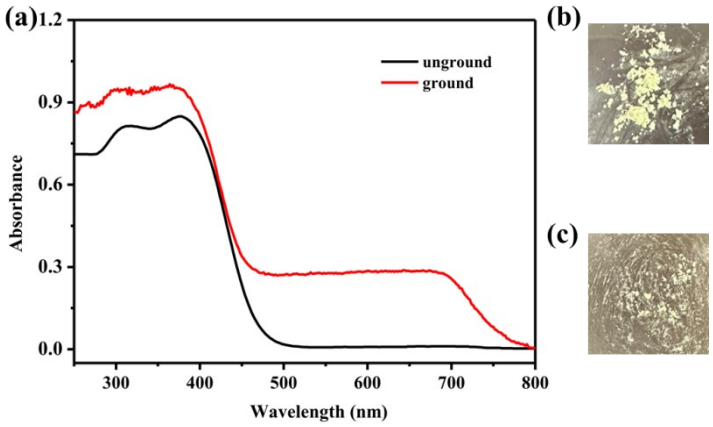

Fig. S9. (a) Solid-state UV-visible absorption spectra of Cu(I) complex **1** before and after grinding. The photographs of solid **1** before (b) and after (c) grinding.

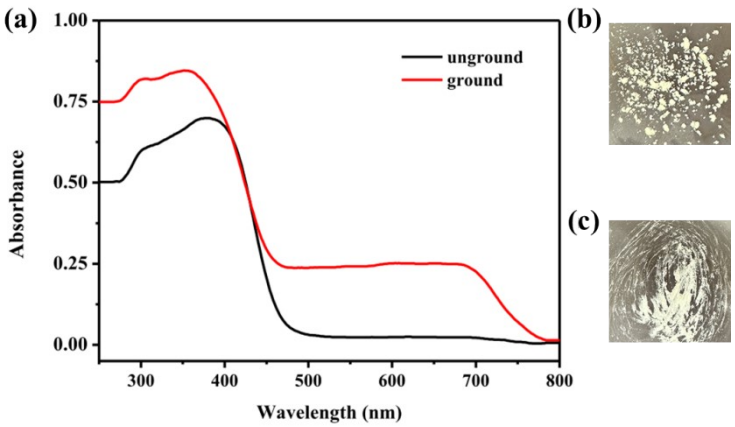

Fig. S10. (a) Solid-state UV-visible absorption spectra of Cu(I) complex **2** before and after grinding. The photographs of solid **2** before (b) and after (c) grinding.

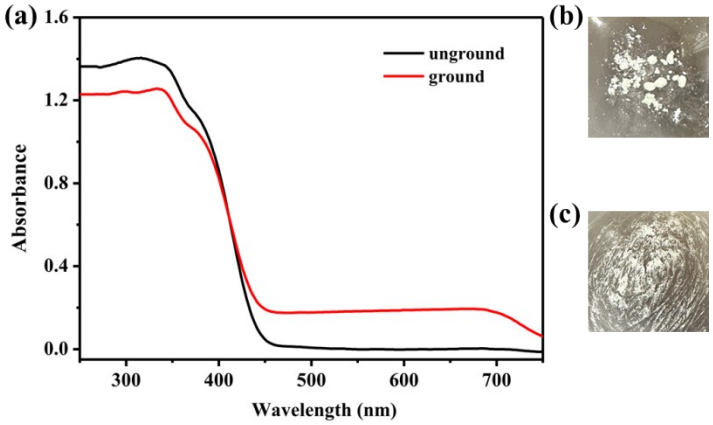

Fig. S11. (a) Solid-state UV-visible absorption spectra of Cu(I) complex **3** before and after grinding. The photographs of solid **3** before (b) and after (c) grinding.

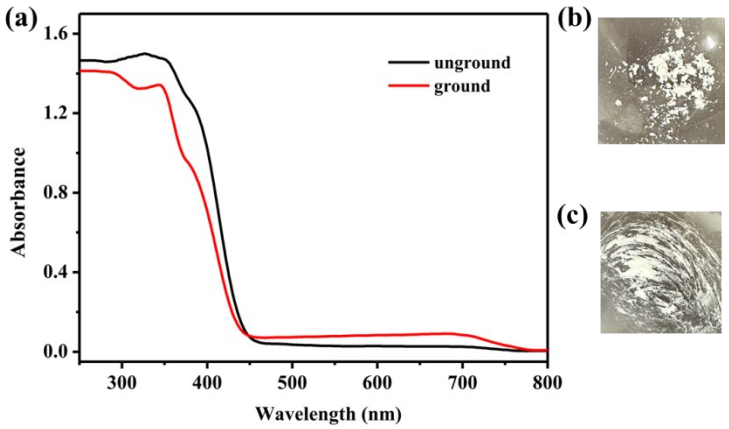

Fig. S12. (a) Solid-state UV-visible absorption spectra of Cu(I) complex **4** before and after grinding. The photographs of solid **4** before (b) and after (c) grinding.

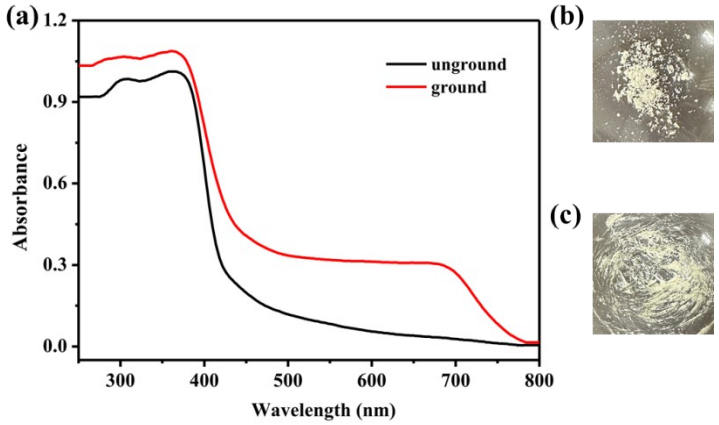

Fig. S13. (a) Solid-state UV-visible absorption spectra of Cu(I) complex **5** before and after grinding. The photographs of solid **5** before (b) and after (c) grinding.

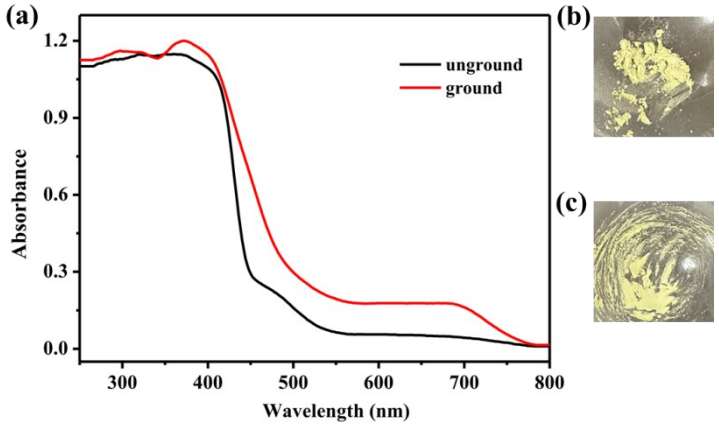

Fig. S14. (a) Solid-state UV-visible absorption spectra of Cu(I) complex **6** before and after grinding. The photographs of solid **6** before (b) and after (c) grinding.

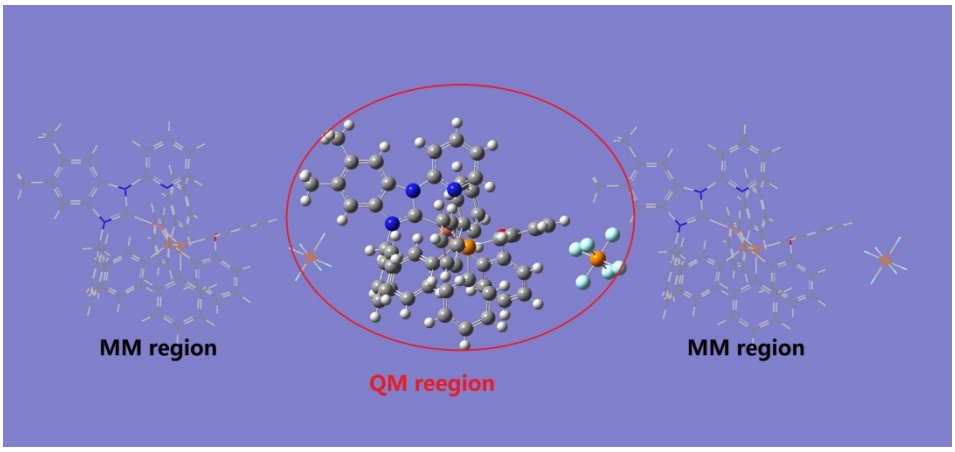

Fig. S15. Setup of QM/MM computational model of Cu(I) complex **2**.

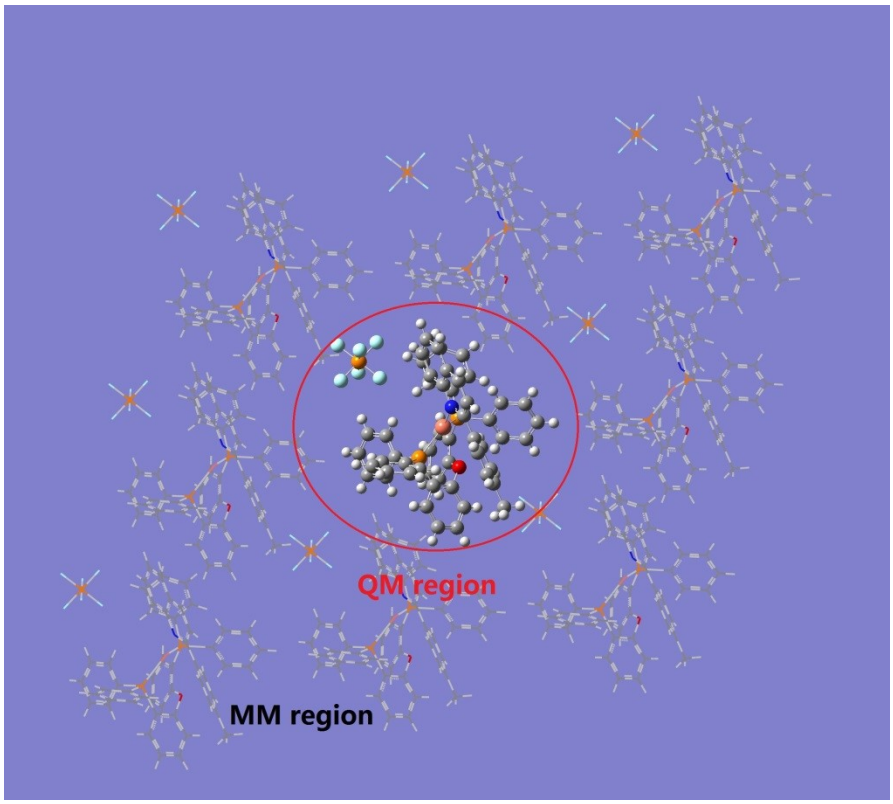

Fig. S16. Setup of QM/MM computational model of Cu(I) complex **4**.

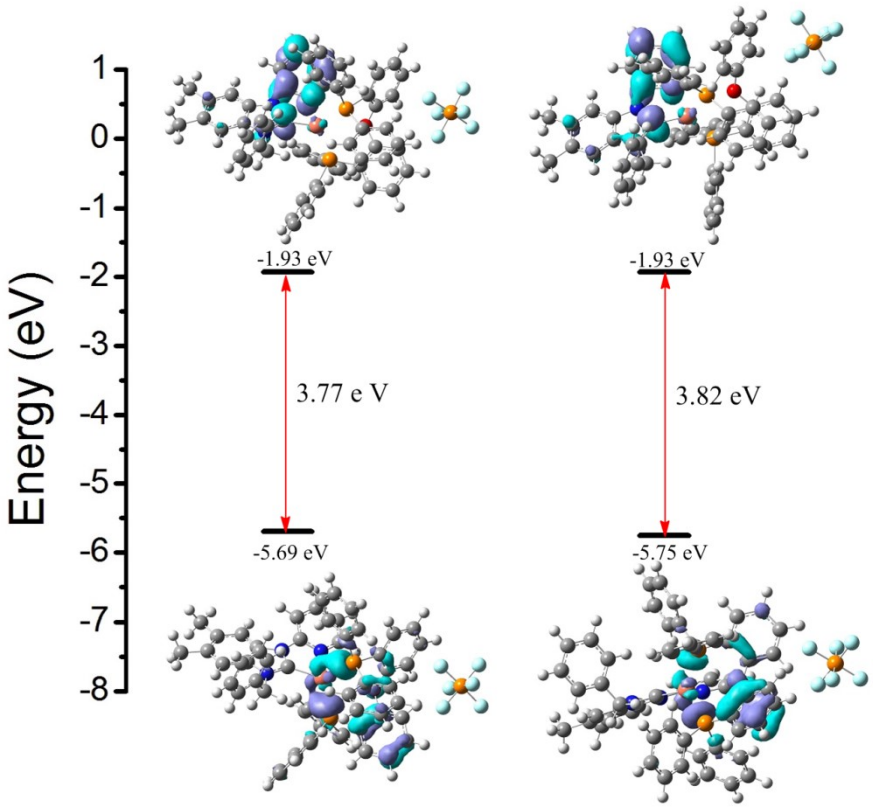

Fig. S17. HOMO and LUMO frontier molecular orbitals of Cu(I) complex **2** in crystalline state (left) and vacuum state (right) calculated using B3LYP/6-31G* basis set.

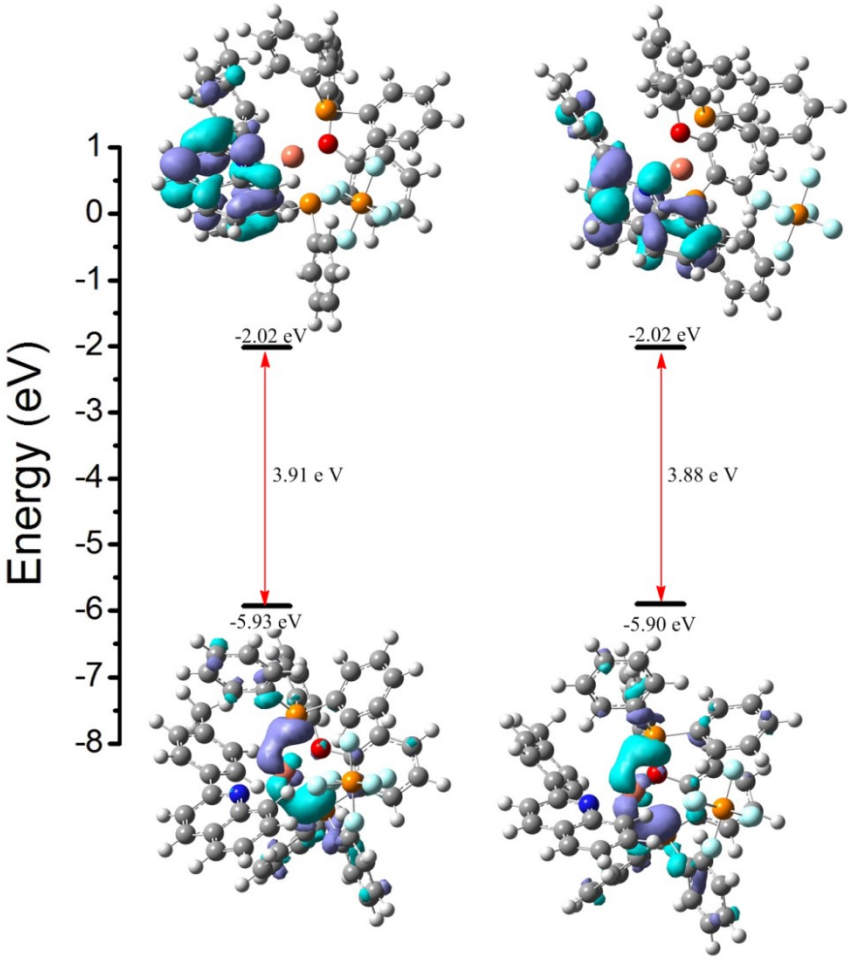

Fig. S18. HOMO and LUMO frontier molecular orbitals of Cu(I) complex **4** in crystalline state (left) and vacuum state (right) calculated using B3LYP/6-31G* basis set.

Table S2. Molecular orbital compositions (%) of HOMO for Cu(I) complex **2** or **4** at different states.

		Contribution (%)		
		Cu	P	Ph
2-HOMO	Crystalline state	43.7		49.4
		22.4	21.3	
	Vacuum state	37.3		55.3
		18.8	18.5	
4-HOMO	Crystalline state	56.9		38.1
		30.7	26.2	
	Vacuum state	57.5		38.4
		30.8	26.7	

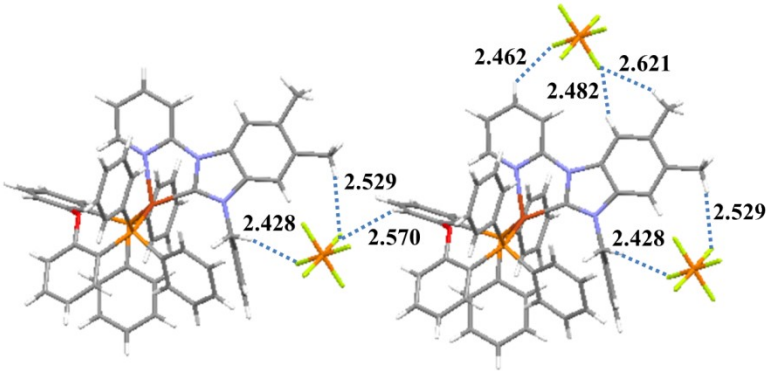

Fig. S19. The structural organization of four-coordinate Cu(I) complex **2**. It showed weak intermolecular C-H···F interactions.

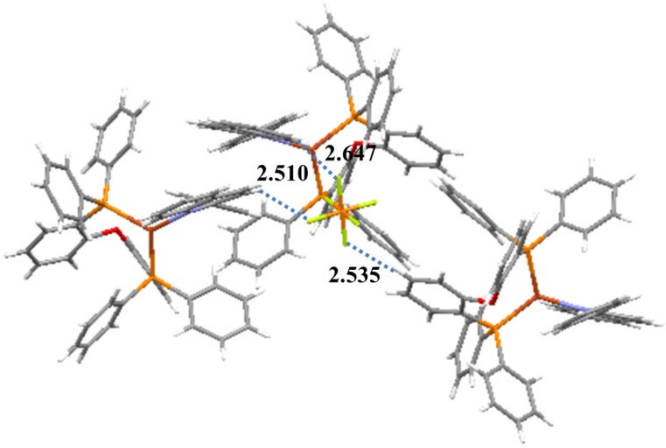

Fig. S20. The structural organization of three-coordinate Cu(I) complex **3**. It showed weak intermolecular C-H···F interactions.

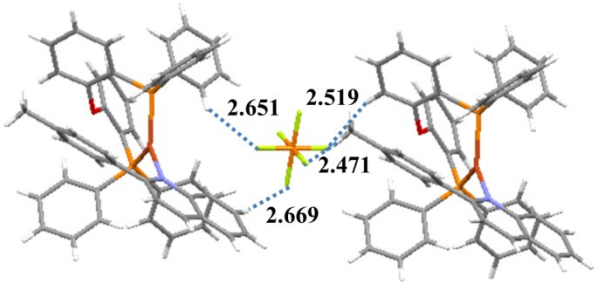

Fig. S21. The structural organization of three-coordinate Cu(I) complex **4**. It showed weak intermolecular C-H···F interactions.

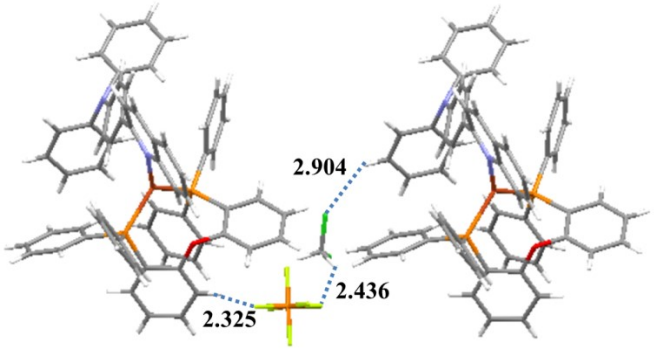

Fig. S22. The structural organization of three-coordinate Cu(I) complex **6**. It showed weak intermolecular C-H···F and C-H···Cl interactions.

Table S3. Structure determination summary for Cu(I) complex **1**.

Empirical formula	$C_{57}H_{46}BrCuN_3OP_2$, F_6P
Formula weight	1139.33
Temperature (K)	193
Crystal system	monoclinic
Space group	P 1 21/n 1
a (Å)	24.8759(12)
b (Å)	16.1720(7)
c (Å)	25.6799(14)
α (deg)	90
β (deg)	99.460(2)
γ (deg)	90
V (Å^3)	10190.4(9)
Z	8
Absorption coefficient (mm^{-1})	1.373
F (000)	4640
Theta range for data collection (deg)	2.33 to 26.10
Index ranges	-29<=h<= 32, -20<=k<= 20, -33<=l<=25
R(reflections)	0.0652(13932)
wR2(reflections)=	0.1249(23296)
Goodness-of-fit on F^2	1.051

Table S4. Structure determination summary for Cu(I) complex **2**.

Empirical formula	$C_{57}H_{47}CuN_3OP_2$, F_6P
Formula weight	1060.42

Temperature (K)	193
Crystal system	monoclinic
Space group	P 1 21/n 1
a (Å)	16.0047(8)
b (Å)	16.1808(7)
c (Å)	19.8413(9)
α (deg)	90
β (deg)	106.624(2)
γ (deg)	90
V (Å^3)	4923.5(4)
Z	4
Absorption coefficient (mm^{-1})	0.609
F (000)	2184
Theta range for data collection (deg)	2.30 to 27.49
Index ranges	-20<=h<= 19, -18<=k<=21, -24<=l<=25
R(reflections)	0.0567(8303)
wR2(reflections)=	0.1171(11283)
Goodness-of-fit on F^2	1.072

Table S5. Structure determination summary for Cu(I) complex **3**.

Empirical formula	$C_{51}H_{39}CuNOP_2$, F_6P
Formula weight	952.28
Temperature (K)	193
Crystal system	monoclinic
Space group	P 1 21/n 1
a (Å)	11.2406(4)
b (Å)	32.1855(13)
c (Å)	13.1783(6)
α (deg)	90
β (deg)	114.2840(10)
γ (deg)	90
V (Å^3)	4345.8(3)
Z	4
Absorption coefficient (mm^{-1})	0.679
F (000)	1952
Theta range for data collection (deg)	2.215 to 26.784
Index ranges	-12<=h<=14, -40<=k<=40, -16<=l<=13

R(reflections)	0.0444(7012)
wR2(reflections)=	0.1101(8918)
Goodness-of-fit on F^2	1.047

Table S6. Structure determination summary for Cu(I) complex **4**.

Empirical formula	$C_{52}H_{41}CuNOP_2$, F_6P
Formula weight	966.31
Temperature (K)	193
Crystal system	triclinic
Space group	P -1
a (Å)	11.2852(5)
b (Å)	13.4528(6)
c (Å)	15.9900(9)
α (deg)	92.554(2)
β (deg)	93.172(2)
γ (deg)	113.872(2)
V (Å^3)	2210.52(19)
Z	2
Absorption coefficient (mm^{-1})	0.669
F (000)	992
Theta range for data collection (deg)	2.215 to 26.784
Index ranges	-14<=h<=14, -17<=k<=17, -20<=l<=18
R(reflections)	0.0539(7355)
wR2(reflections)=	0.1154(10075)
Goodness-of-fit on F^2	1.037

Table S7. Structure determination summary for Cu(I) complex **6**.

Empirical formula	$C_{63}H_{48}CuN_2OP_2$, F_6P, CH_2Cl_2
Formula weight	1204.41
Temperature (K)	193
Crystal system	triclinic
Space group	P -1
a (Å)	13.9127(8)
b (Å)	14.3328(7)
c (Å)	15.2579(8)
α (deg)	72.526(2)
β (deg)	75.888(2)

γ (deg)	82.441(2)
V (Å^3)	2809.0(3)
Z	2
Absorption coefficient (mm^{-1})	0.635
F (000)	1236
Theta range for data collection (deg)	1.845 to 27.430
Index ranges	-17<=h<=18, -18<=k<=18, -19<=l<=19
R(reflections)	0.0649(8349)
wR2(reflections)=	0.1699(12748)
Goodness-of-fit on F^2	1.015

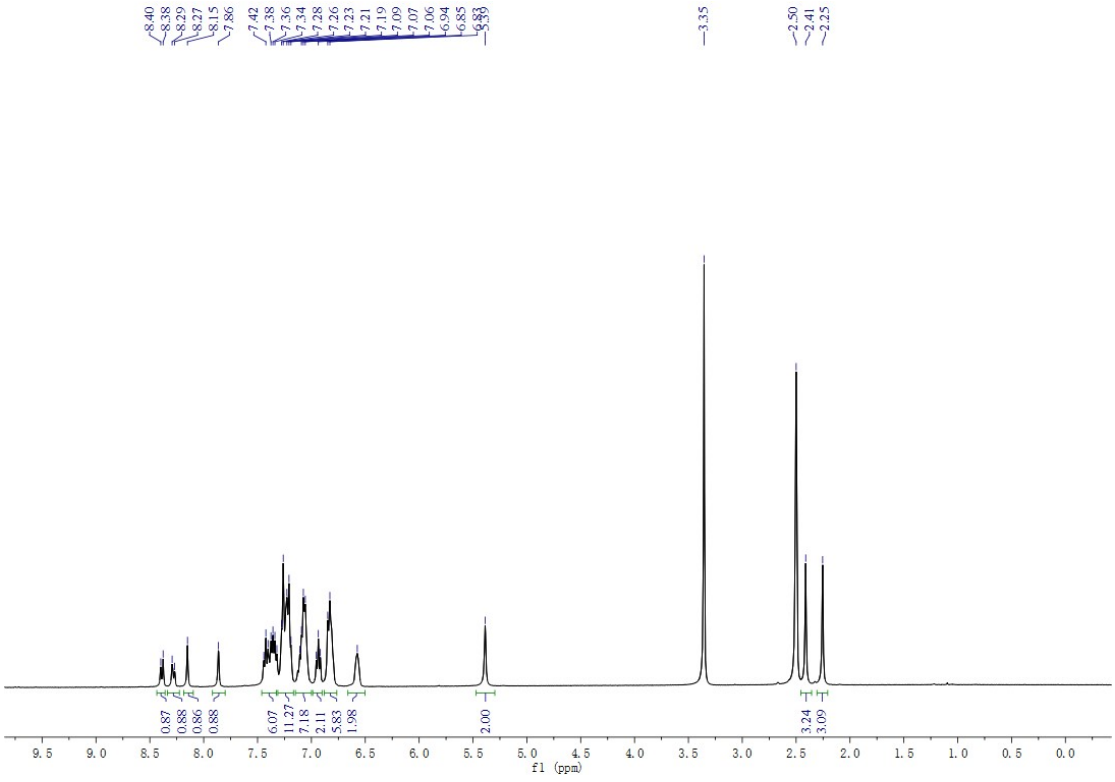

Fig. S23. The ^{1}H NMR spectroscopy of **1**.

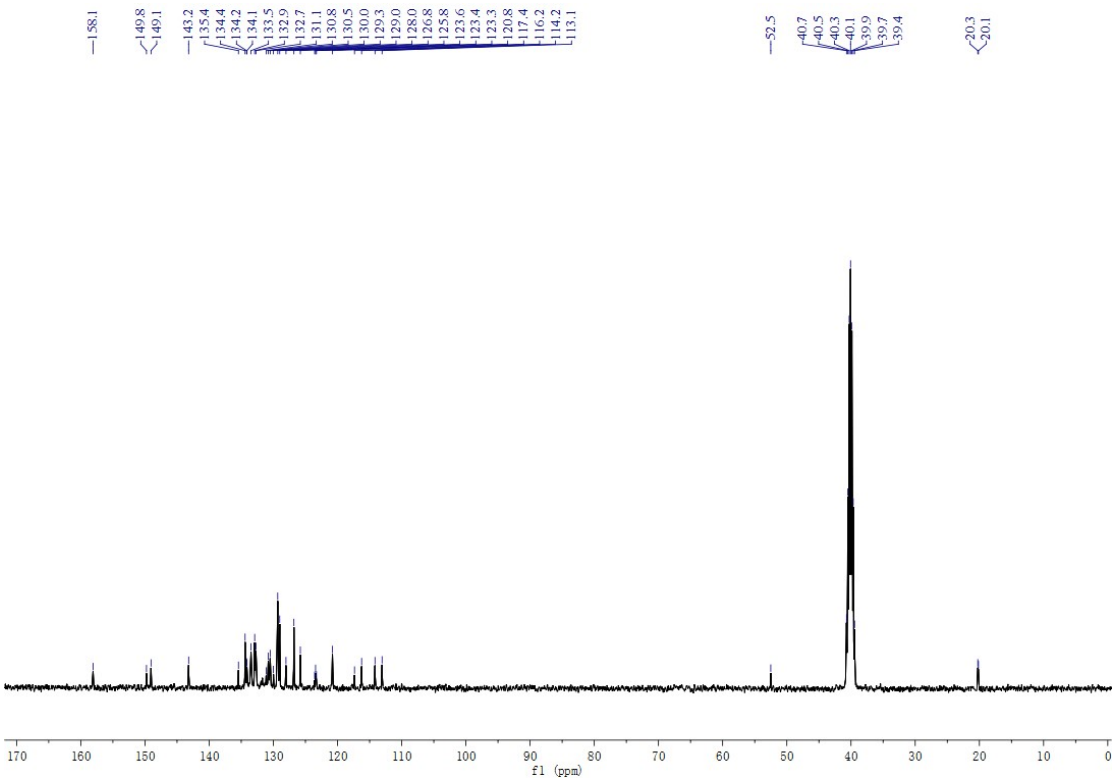

Fig. S24. The ^{13}C NMR spectroscopy of **1**.

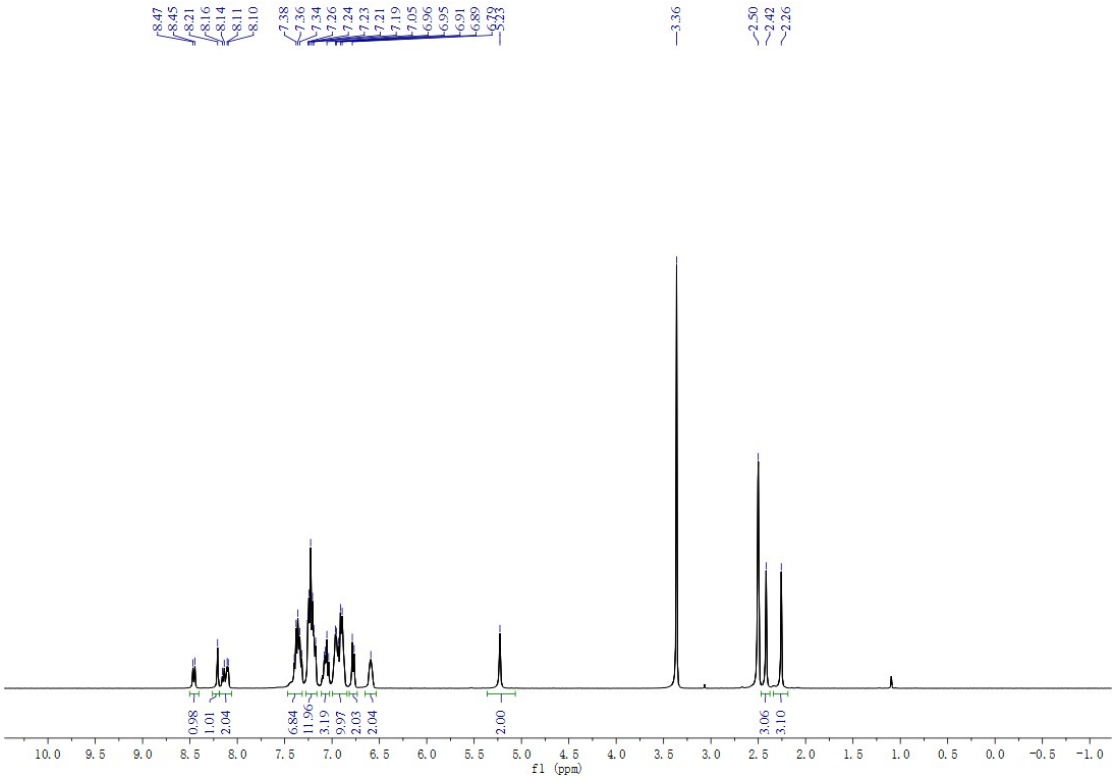

Fig. S25. The ^{1}H NMR spectroscopy of **2**.

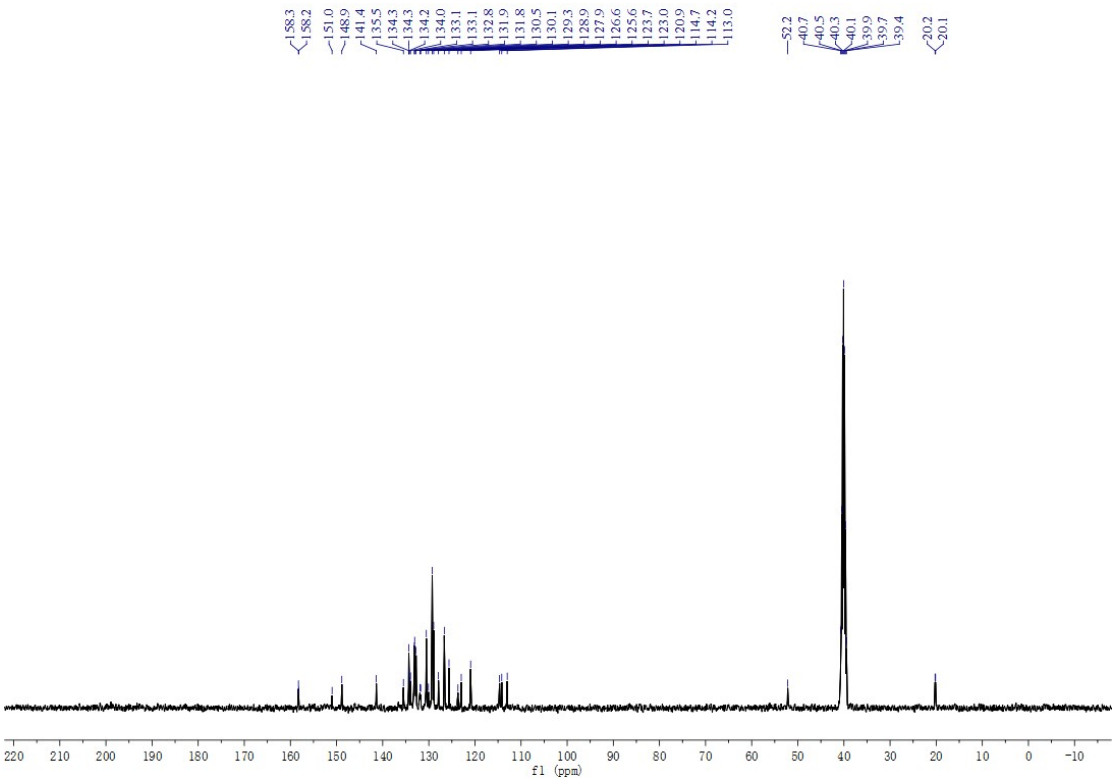

Fig. S26. The ^{13}C NMR spectroscopy of **2**.

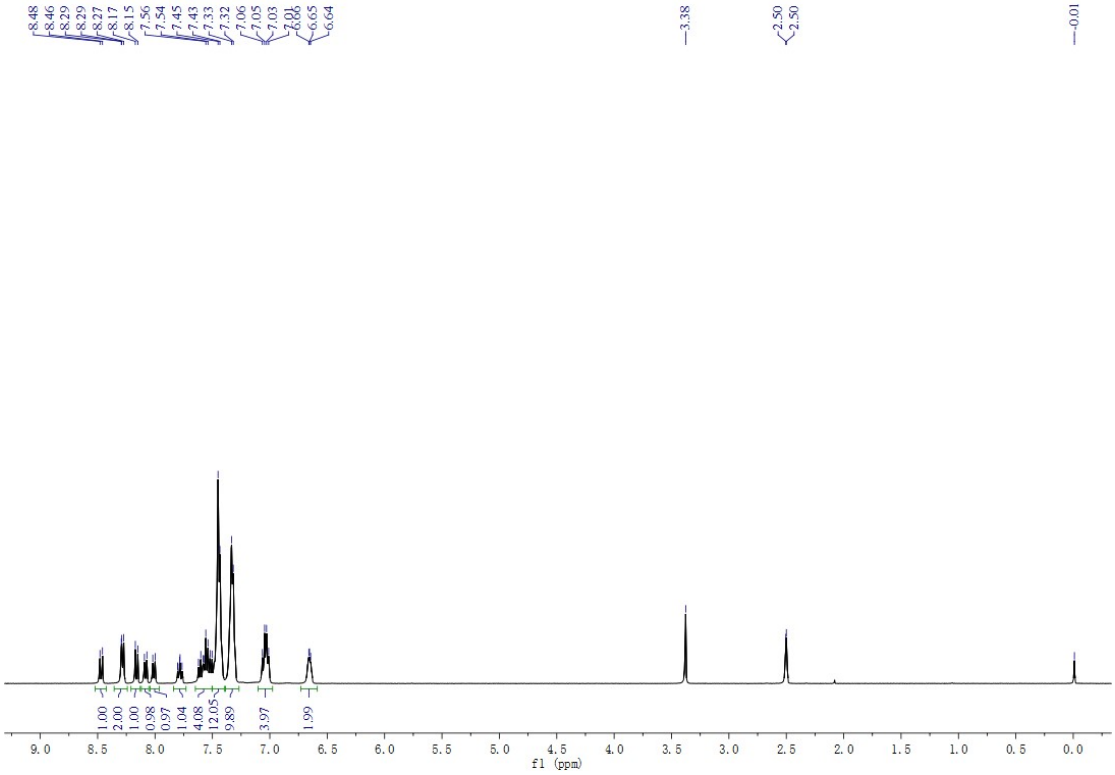

Fig. S27. The ^{1}H NMR spectroscopy of **3**.

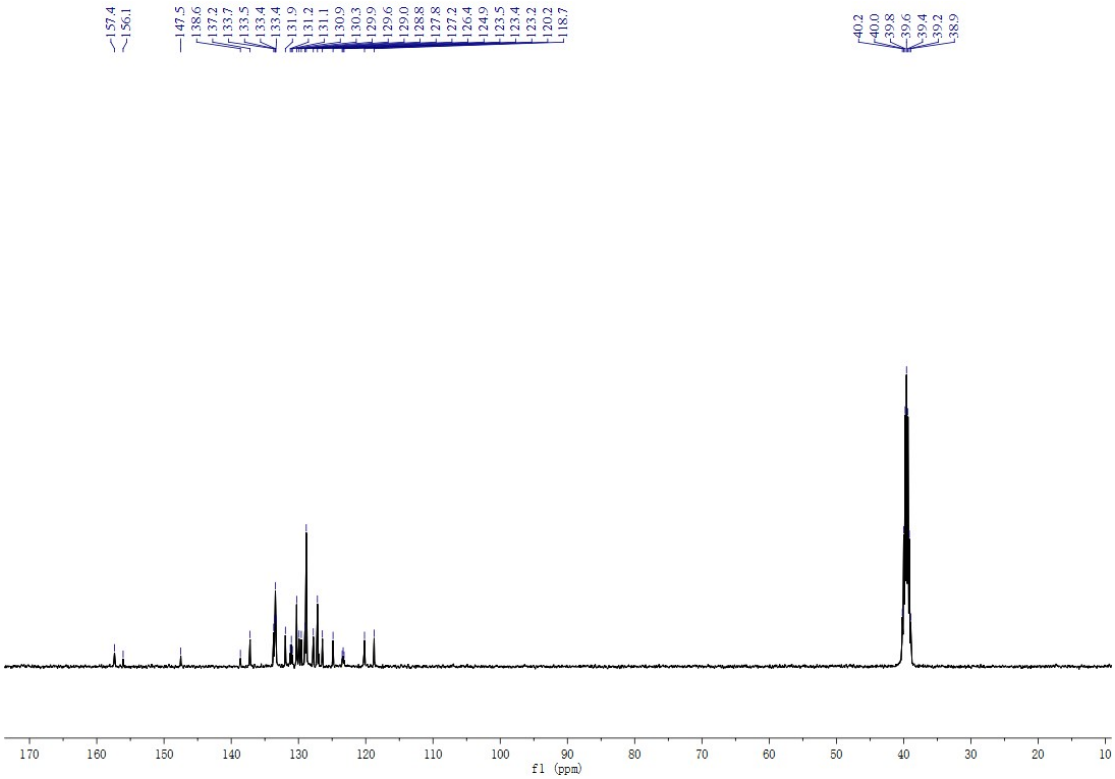

Fig. S28. The ^{13}C NMR spectroscopy of **3**.

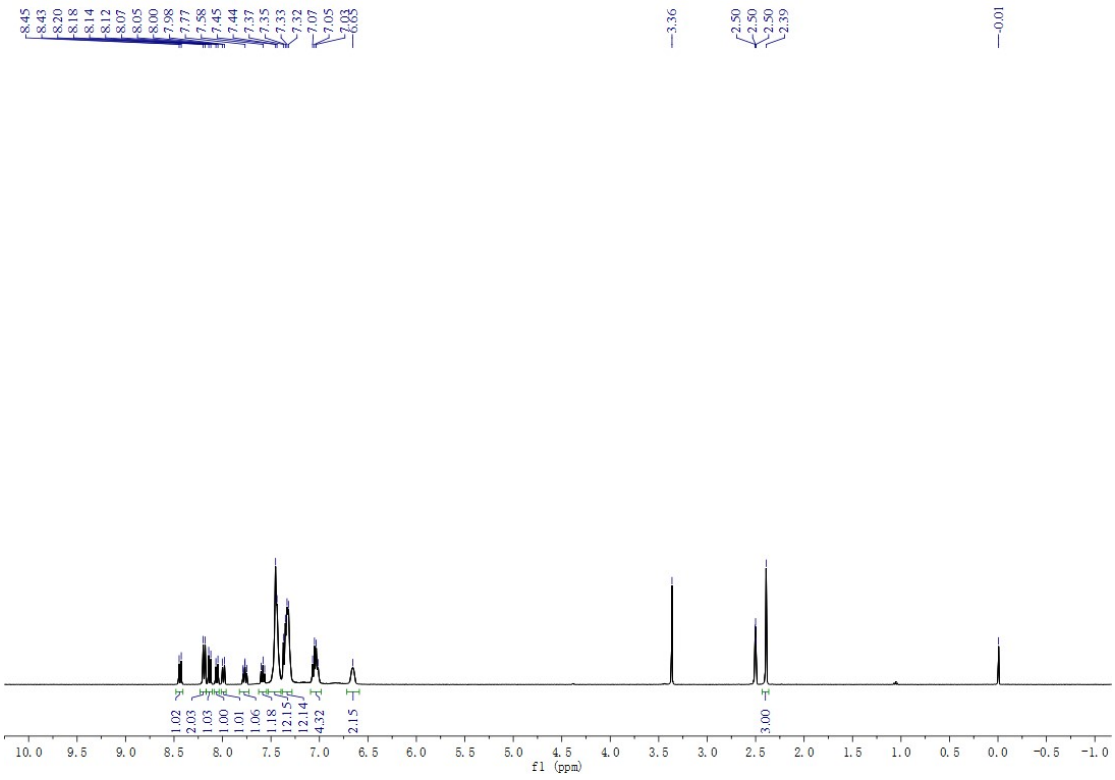

Fig. S29. The ^{1}H NMR spectroscopy of **4**.

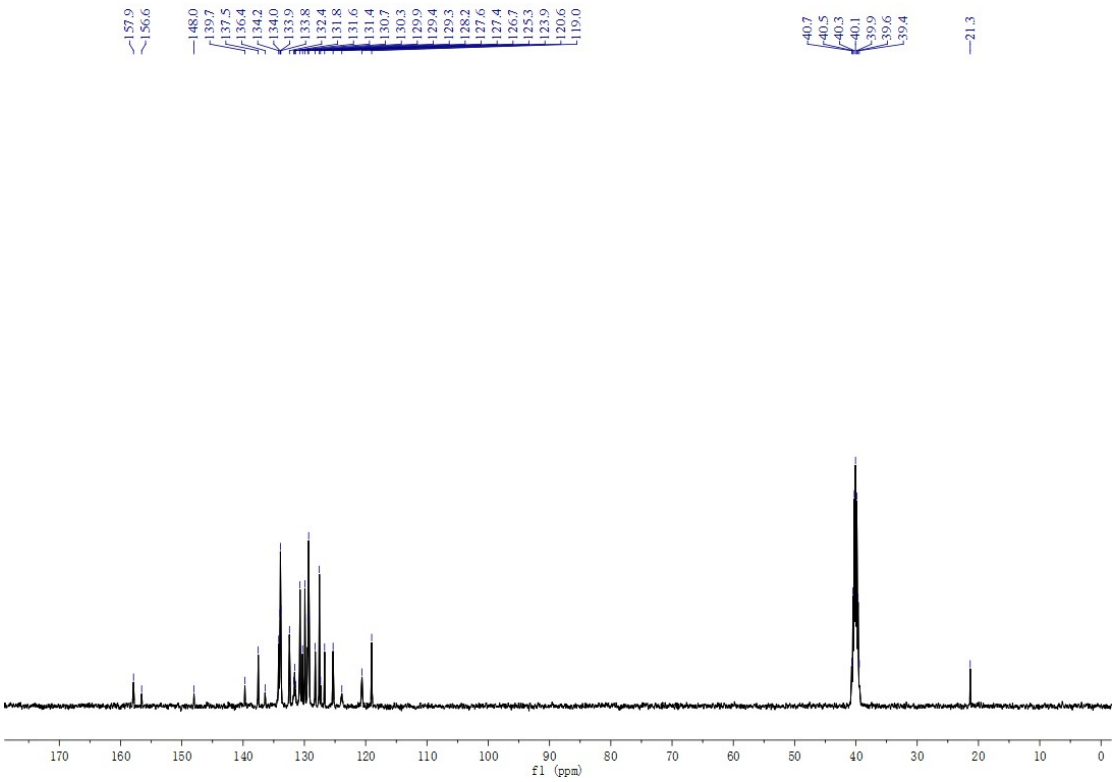

Fig. S30. The ^{13}C NMR spectroscopy of **4**.

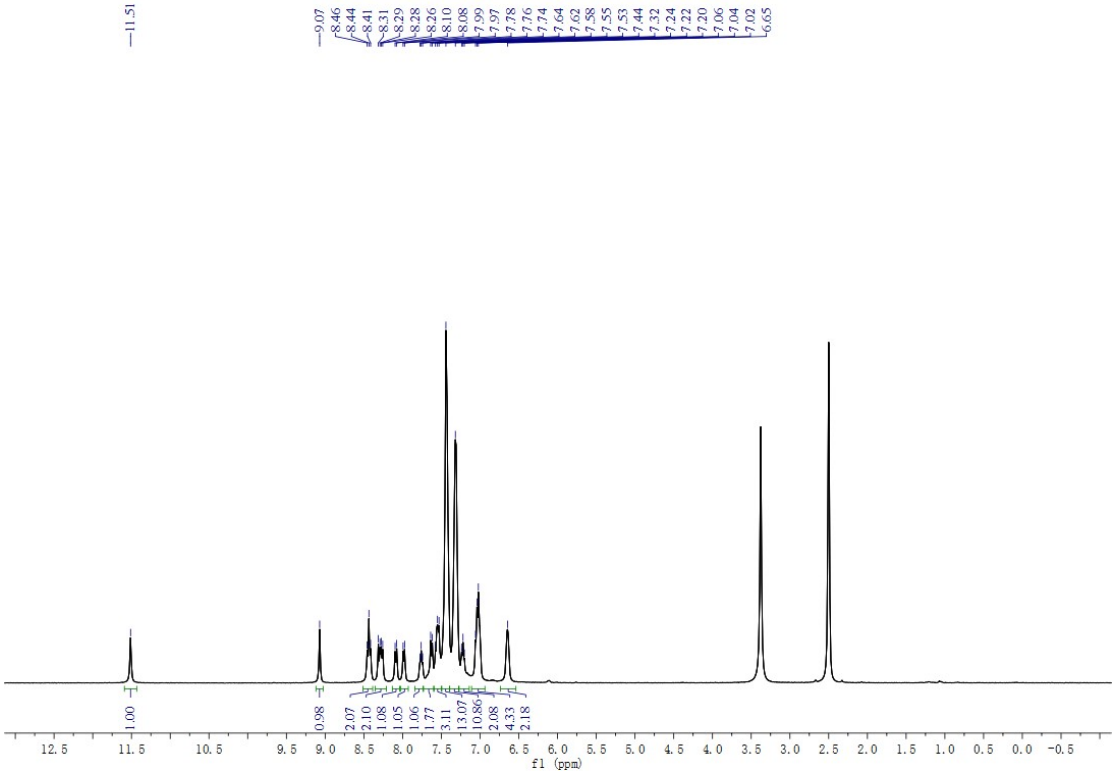

Fig. S31. The ^{1}H NMR spectroscopy of **5**.

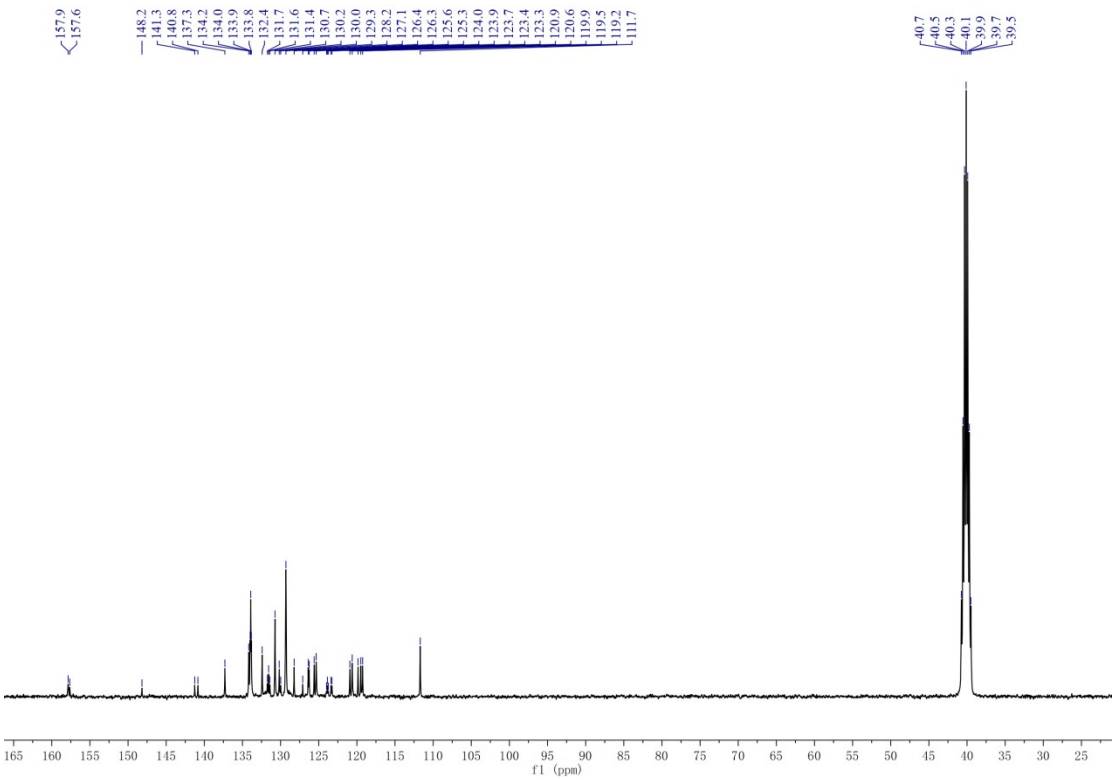

Fig. S32. The ^{13}C NMR spectroscopy of **5**.

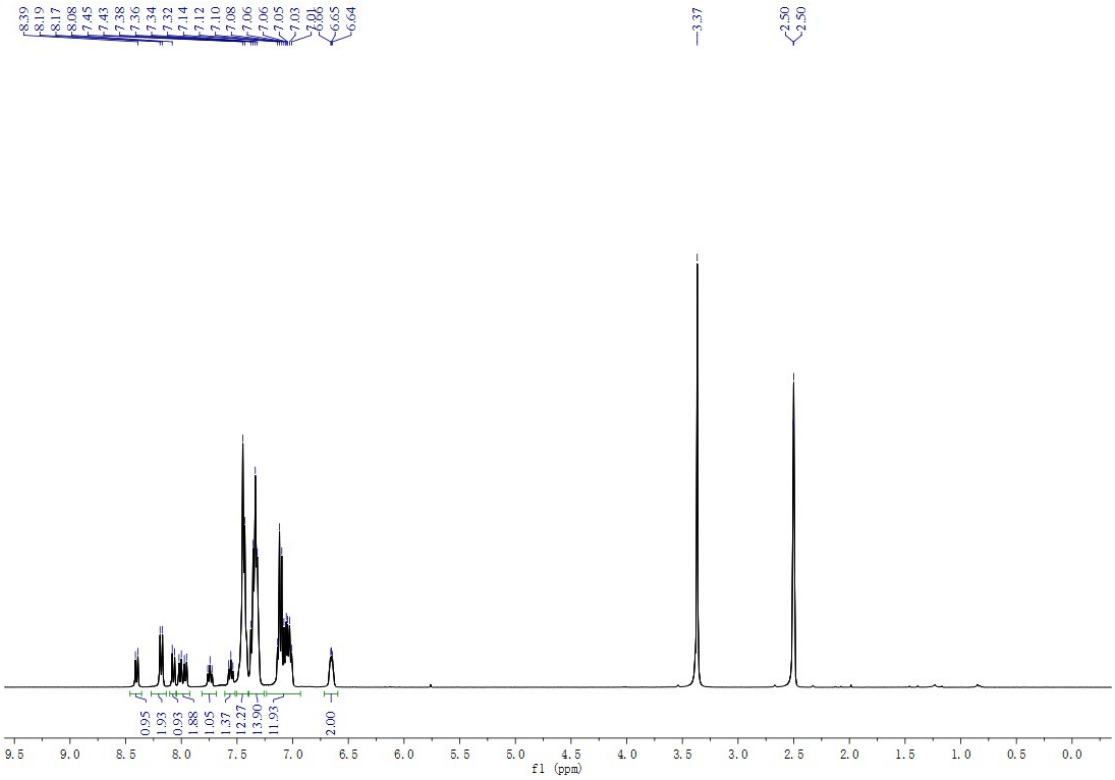

Fig. S33. The ^{1}H NMR spectroscopy of **6**.

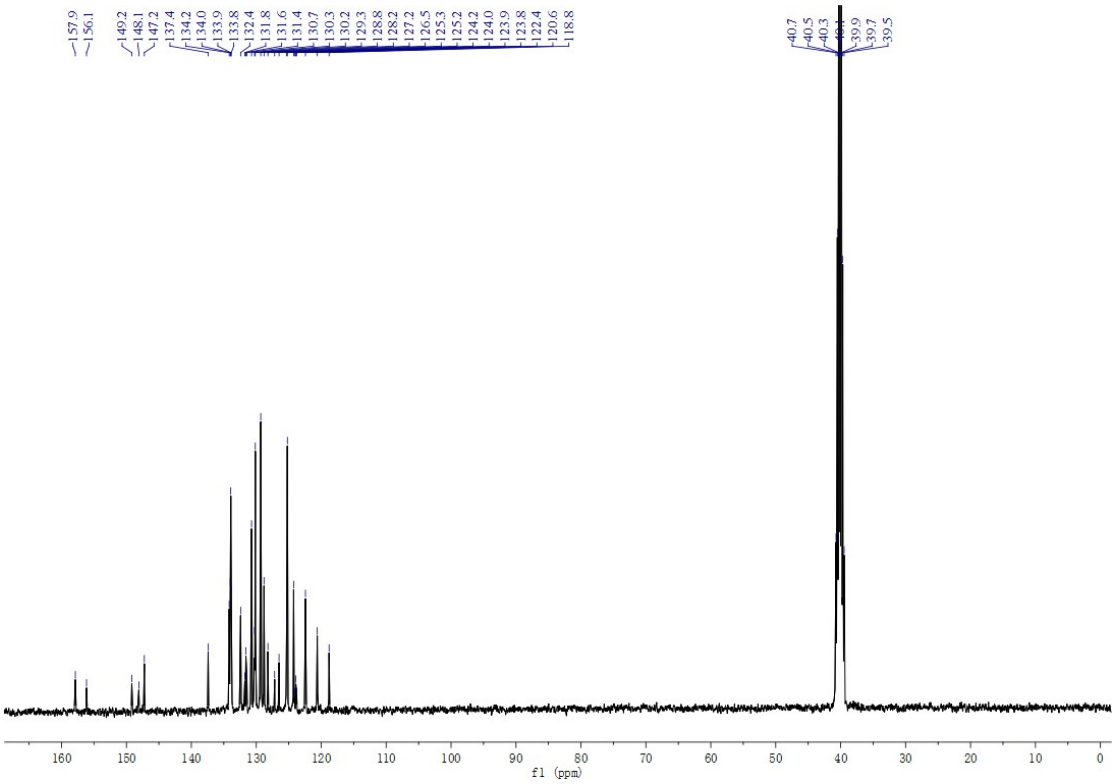

Fig. S34. The ^{13}C NMR spectroscopy of **6**.